Intrinsic connectivity networks in healthy subjects explain clinical variability in Alzheimer's disease

Manja Lehmann[a,b,c,1], Cindee M. Madison[b], Pia M. Ghosh[a,b], William W. Seeley[a], Elizabeth Mormino[b], Michael D. Greicius[d], Maria Luisa Gorno-Tempini[a], Joel H. Kramer[a], Bruce L. Miller[a], William J. Jagust[a,b,e], and Gil D. Rabinovici[a,b,e]

[a]Memory and Aging Center, Department of Neurology, University of California, San Francisco, CA 94158; [b]Helen Wills Neuroscience Institute, University of California, Berkeley, CA 94720; [c]Dementia Research Centre, Institute of Neurology, University College London, London WC1N 3BG, United Kingdom; [d]Functional Imaging in Neuropsychiatric Disorders Laboratory, Department of Neurology and Neurological Sciences, Stanford University School of Medicine, Stanford, CA 94305; and [e]Lawrence Berkeley National Laboratory, Berkeley, CA 94720

Edited by Marcus E. Raichle, Washington University in St. Louis, St. Louis, MO, and approved May 28, 2013 (received for review January 6, 2013)

Although previous studies have emphasized the vulnerability of the default mode network (DMN) in Alzheimer's disease (AD), little is known about the involvement of other functional networks and their relationship to clinical phenotype. To test whether clinicoanatomic heterogeneity in AD is driven by the involvement of specific networks, network connectivity was assessed in healthy subjects by seeding regions commonly and specifically atrophied in three clinical AD variants: early-onset AD (age at onset, <65 y; memory and executive deficits), logopenic variant primary progressive aphasia (language deficits), and posterior cortical atrophy (visuospatial deficits). Four-millimeter seed regions of interest were used to obtain intrinsic connectivity maps in 131 healthy controls (age, 65.5 ± 3.5 y). Atrophy patterns in independent cohorts of AD variant patients and their correspondence to connectivity networks in controls were also assessed. The connectivity maps of commonly atrophied regions of interest support posterior DMN and precuneus network involvement across AD variants, whereas seeding regions specifically atrophied in each AD variant revealed distinct, syndrome-specific connectivity patterns. Goodness-of-fit analysis of each connectivity map with network templates showed the highest correspondence between the early-onset AD seed connectivity map and anterior salience and right executive-control networks, the logopenic aphasia seed connectivity map and the language network, and the posterior cortical atrophy seed connectivity map and the higher visual network. Connectivity maps derived from controls matched regions commonly and specifically atrophied in the patients. Our findings indicate that the posterior DMN and precuneus network are commonly affected in AD variants, whereas syndrome-specific neurodegenerative patterns are driven by the involvement of specific networks outside the DMN.

Alzheimer's disease (AD) is a progressive neurodegenerative disorder characterized by extracellular accumulation of amyloid plaques, intracellular neurofibrillary tangles, and neuronal loss (1). Although most patients present with memory deficits, a significant minority of patients with AD present with nonamnestic syndromes (2, 3). Patients with nonfamilial early-onset AD (EOAD, defined as onset <65 y in most studies) often show heterogeneous cognitive deficits, including impairment in attention and executive functions (4, 5). Focal syndromes such as posterior cortical atrophy (PCA, characterized by predominant visuospatial and visuoperceptual deficits; ref. 6) and the logopenic variant of primary progressive aphasia [lvPPA, a progressive disorder of language (7, 8)] are also most commonly caused by AD pathology. It has been suggested that up to 15% of patients with AD seen in dementia centers have nonamnestic presentations (2), and the importance of these syndromes is reflected in their inclusion in new diagnostic guidelines for AD (9, 10). The factors driving the clinicoanatomical heterogeneity in AD are not well understood. One possible mechanism that could explain the specific involvement of different brain regions in AD variants is the spread of disease via distinct functional networks.

Recent advances in functional neuroimaging have provided important insights into the dysfunction of large-scale neural networks in neurodegenerative diseases. Studies using task-free (resting-state) functional magnetic resonance imaging (fMRI) data have shown that correlated spontaneous activity occurs between functionally related brain regions (11, 12). Disease-specific atrophy patterns have been shown to closely match intrinsic connectivity maps in cognitively normal individuals, suggesting that neurodegenerative disorders target specific functional networks in the human brain (13, 14). This observation is consistent with in vitro and in vivo studies in animal models showing that disease-associated protein aggregates spread via interconnected neural networks (15–17). Functional connectivity studies have further provided evidence for a core network, commonly referred to as the default mode network (DMN), that is particularly vulnerable and affected in AD (18, 19). Changes in DMN connectivity are detected even in the preclinical stages of AD (20, 21) and distinguish AD from other neurodegenerative diseases (22). Although the behavioral correlates of the DMN remain to be characterized in more detail, it has been hypothesized that the DMN plays a role in attending to both internally and externally generated environmental stimuli (23, 24). The DMN has been further divided into two to three functional subnetworks: a ventral component (including retrosplenial cortex and medial temporal lobe) and a dorsal component that can be further divided into anterior (prefrontal-predominant) and posterior (parietal-predominant) modules (25).

Little is currently known about the dysfunction of the DMN and other networks in atypical clinical variants of AD. A recent positron emission tomography (PET) study showed that patterns of glucose hypometabolism in EOAD, lvPPA, and PCA matched the network templates of executive-control, language, and visual networks, respectively (26), suggesting that the clinical phenotype in AD may be driven by the relative involvement of functional networks outside the DMN. Structural MRI studies, in contrast, have shown that patterns of neurodegeneration converge in the DMN in different variants of AD (27, 28), suggesting that the DMN may represent a core network that is commonly affected across AD variants. These data are consistent with a model in which AD pathology spreads from the DMN to closely interconnected posterior networks, including those involved in visuospatial, language, and executive function, or conversely, that

Author contributions: M.L., W.W.S., E.M., and G.D.R. designed research; M.L. and P.M.G. performed research; M.L., C.M.M., M.D.G., and W.J.J. contributed new reagents/analytic tools; M.L. analyzed data; J.H.K. recruited and assessed subjects; and M.L., C.M.M., P.M.G., W.W.S., E.M., M.D.G., M.L.G.-T., J.H.K., B.L.M., W.J.J., and G.D.R. wrote the paper.

The authors declare no conflict of interest.

This article is a PNAS Direct Submission.

[1]To whom correspondence should be addressed. E-mail: mlehmann@memory.ucsf.edu.

This article contains supporting information online at www.pnas.org/lookup/suppl/doi:10.1073/pnas.1221536110/-/DCSupplemental.

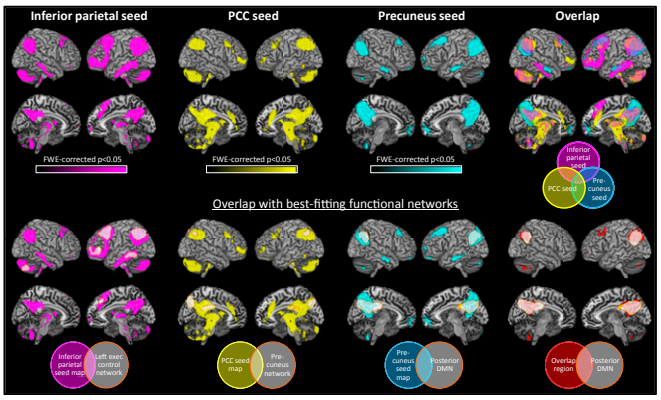

Fig. 1. Task-free intrinsic connectivity network maps in healthy individuals produced by seeding three regions that were commonly atrophied in AD variants, as well as the overlap of the three connectivity maps. Shown are statistical *P* maps after correction for multiple comparisons (FWE, $P < 0.05$). Bottom panel also shows the overlap of each connectivity map as well as the overlap region between the three maps with the best-fitting network templates, as revealed by GOF analysis.

neurodegeneration in AD begins in more peripheral networks in clinical variants of AD and converges in the DMN across variants.

In this study, we aimed to assess intrinsic connectivity networks in the healthy brain by seeding regions of interest (ROIs) demonstrated in a previous study to be either commonly or specifically atrophied in three AD variants: EOAD, lvPPA, and PCA. These variants, although less common than typical late-onset amnestic AD, were selected to maximize the heterogeneity of clinical phenotype and degenerative pattern. We hypothesized that seeding regions commonly atrophied in AD variants (i.e., peak atrophy voxels across all syndromes compared with controls) will produce similar network maps in healthy controls and may point toward functional networks commonly affected in all three AD variants. In contrast, seeding regions specifically atrophied in AD variants (i.e., peak atrophy voxels in each syndrome compared with the other two) will produce distinct network connectivity maps in the healthy brain and may point to networks that are specifically affected in the different variants. To assess the overlap of the resulting connectivity maps with published network templates, a goodness-of-fit analysis was conducted, testing each connectivity map against a set of 15 functional network templates (refs. 25 and 29 and http://findlab.stanford.edu/functional_ROIs.html). To ascertain the relevance of the connectivity patterns detected in controls to disease, we compared the connectivity patterns from common and syndrome-specific ROIs to regions commonly and specifically atrophied in an independent sample of patients with the three AD variants, as assessed using voxel-based morphometry (VBM). A flowchart summarizing the experimental procedures conducted in this study is presented in Fig. S1.

Results

Network Connectivity Maps. ***Commonly atrophied regions.*** Peak atrophy voxels found in all three AD variants compared with controls (identified in a previous VBM study, ref. 28) included the left inferior parietal lobule, left posterior cingulate cortex (PCC), and left precuneus (Fig. S2). As shown in Fig. 1, intrinsic connectivity maps produced by seeding these three ROIs in 131 healthy individuals are very similar. Maps of all three seeds include lateral parietal (in particular angular gyrus) and medial parietal (precuneus) regions, posterior cingulate cortex, and dorsolateral prefrontal regions. The inferior parietal and PCC ROI connectivity maps also showed involvement of large parts of the brainstem and cerebellum, as well as thalamus and striatum. The goodness-of-fit (GOF) analysis revealed that the inferior parietal seed connectivity map fit best with the left executive-control network (GOF, 13.37; see Table S1 for complete overview of GOF results), closely followed by the posterior DMN (GOF, 12.48); the connectivity map of the PCC seed fit best with the precuneus network (GOF, 11.75), again closely followed by the posterior DMN (GOF, 10.48); and the precuneus seed connectivity map fit best with the posterior DMN (GOF, 12.76), followed by the precuneus network template (GOF, 10.57). It is noteworthy that the GOF scores between the first and second fits were very similar. There was 41% overlap between any two maps and a 14% overlap of all three maps (Fig. 1). All three maps overlapped in bilateral angular gyrus, precuneus, PCC, and dorsolateral prefrontal cortex. These regions of overlap between the three connectivity maps showed the highest GOF index with the posterior DMN template (GOF, 27.11), closely followed by the precuneus network (GOF, 21.12).

Specifically atrophied regions. Peak atrophy voxels identified on VBM in the distinct AD variants (each variant compared with the other two) were the right middle frontal gyrus in EOAD, left superior temporal sulcus in lvPPA, and right middle occipital gyrus in PCA (Fig. S2). Seeding these three seed ROIs in healthy individuals produced distinct connectivity maps that demonstrated remarkable overlap with networks associated with the predominant cognitive deficits seen in each syndrome.

The network connectivity map produced by seeding the EOAD seed ROI included mainly bilateral (right more than left) dorsolateral prefrontal cortex, frontal pole, anterior insula, anterior cingulate, and inferior and superior parietal lobe (Fig. 2). The GOF analysis revealed two strong fits: the highest fit was found with the anterior salience network, and the second-best fit was found with the right executive-control network, with only a small difference in GOF scores between both fits (GOF, 6.73 and 6.43, respectively). Reviewing the overlap of the EOAD seed ROI connectivity map with the network templates (Fig. 3) revealed that the fit with the anterior salience network is particularly strong in the left hemisphere, whereas the connectivity patterns in the right hemisphere overlap better with the right executive-control network. Indeed, splitting the EOAD seed ROI correlation map into

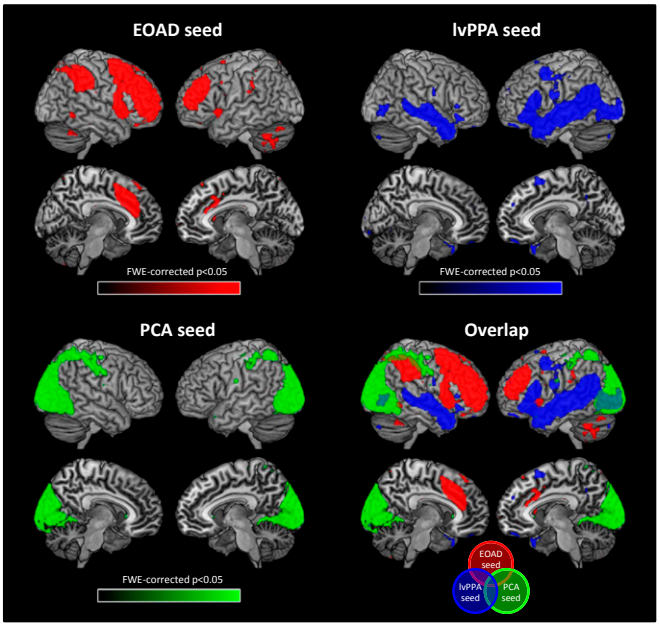

Fig. 2. Task-free intrinsic connectivity network maps in healthy individuals produced by seeding three regions that were specifically atrophied in AD variants. Shown are statistical *P* maps after correction for multiple comparisons (FWE, $P < 0.05$).

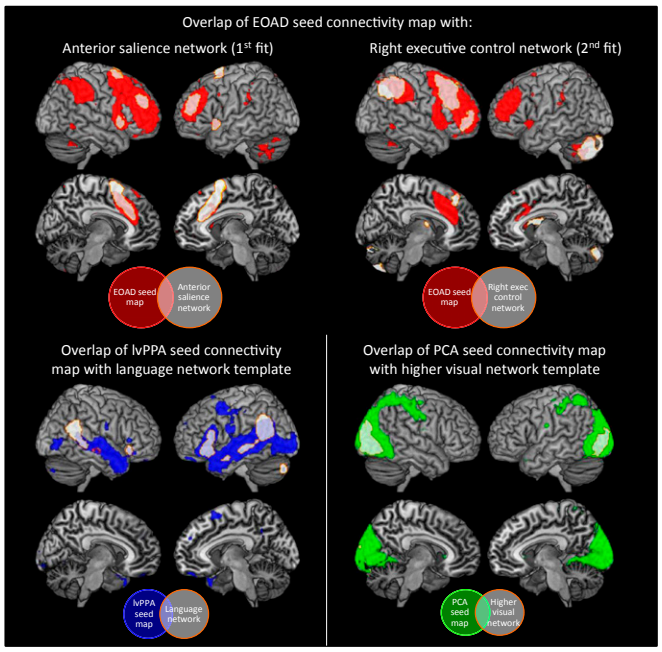

Fig. 3. Overlap of seed-based connectivity networks of specifically atrophied ROIs with best-fitting functional network templates. The EOAD seed connectivity map showed two strong fits: the anterior salience network showed the best fit with the left hemisphere connectivity map, and the right executive-control network showed the best fit with the right connectivity map. The lvPPA seed and PCA seed connectivity maps showed the best fit with the language and higher visual networks, respectively.

left- and right-hemisphere components confirmed that the highest fit for the right-sided connectivity patterns is with the right executive-control network, and the best fit for the left hemisphere map is with the anterior salience network.

The network connectivity map of the lvPPA seed ROI involved bilateral (left more than right) middle and superior temporal gyri and the inferior parietal lobule, with some involvement of left inferior and middle frontal gyri (Fig. 2). The GOF analysis showed the highest fit with the language network template (GOF, 7.94, Fig. 3), whereas the second-best fit (with the higher visual network) was much weaker (GOF, 3.54). The network connectivity map produced by the PCA seed ROI involved mainly bilateral lateral and medial occipital lobe regions, extending anteriorly into the fusiform gyrus and the superior parietal lobe (Fig. 2). The GOF analysis revealed the best fit with the higher visual network (GOF, 13.26, Fig. 3), and the second-best fit with the primary visual network (GOF, 6.13). The overlap map showed that there was very little overlap between the three connectivity maps, with 3% overlap of any two maps and no regions in which all three maps overlapped (Fig. 2).

Atrophy Patterns. Regions atrophied in each AD variant compared with controls are shown in Fig. 4. EOAD patients showed gray matter atrophy bilaterally in the precuneus, posterior parietal lobe, posterior cingulate gyrus, middle and superior temporal gyrus, medial temporal lobe structures including the hippocampus, superior frontal gyrus, and thalamus. In contrast, patients with lvPPA showed asymmetric (L > R) atrophy in lateral temporal regions (inferior, middle, and superior), as well as posterior parietal and lateral occipital lobes. Patients with PCA showed predominant posterior involvement, with atrophy bilaterally in the occipital and posterior parietal lobes, precuneus, posterior cingulate gyrus, and inferior and middle temporal gyrus. There was 50% overlap between any two maps, and 17% where all three comparisons overlapped, which included the posterior parietal lobe and inferior and middle temporal gyrus. The overlap in posterior brain regions matches the posterior involvement of the connectivity maps for the commonly atrophied ROIs (Fig. 1).

Regions that were specifically atrophied in EOAD compared with the other two variants were the bilateral orbitofrontal and superior frontal gyrus, left precuneus, and right medial temporal lobe (Fig. 4). In contrast, patients with lvPPA were specifically atrophied in left superior and middle temporal gyrus, as well as the left temporal pole. Patients with PCA were specifically atrophied in bilateral occipital lobe regions, as well as superior parietal lobe and precuneus. The involvement of frontal regions in EOAD, left temporoparietal regions in lvPPA, and bilateral occipitoparietal regions in PCA overlap with the same regions in the respective network connectivity maps in the healthy controls (Fig. 2).

Discussion

In this study, we assessed intrinsic connectivity networks in the healthy brain by seeding regions that were commonly and specifically atrophied in different clinical variants of AD: an amnestic/dysexecutive variant (EOAD), a language variant (lvPPA), and a visual variant (PCA). We hypothesized that seeding the common ROIs in healthy controls would reveal core networks affected in AD regardless of clinical presentation, whereas seeding regions that are distinctly atrophied in EOAD, lvPPA, and PCA would identify networks that are uniquely affected in each syndrome and correspond to the clinical deficits. We further hypothesized that the networks extracted from the common ROIs in controls would overlap with regions of common atrophy across AD variants, whereas networks extracted from syndrome-specific ROIs would correspond with variant-specific atrophy in patients. Interestingly, the connectivity maps derived from commonly atrophied regions point to a strong involvement of the posterior DMN and the precuneus network. The individual connectivity maps produced by commonly affected seed ROIs as well as the overlap region between the three maps showed strong fits with the posterior default mode/precuneus networks, suggesting that these networks may be commonly affected across different AD variants. These regions greatly overlap with regions atrophied in all three AD variants compared with controls in our VBM analysis. In striking contrast, seeding regions specifically atrophied in different AD variants produced distinct and syndrome-specific connectivity maps that matched the clinical phenotypes and showed little overlap with one another. These connectivity maps, however, greatly overlapped with regions specifically atrophied in each variant, as shown

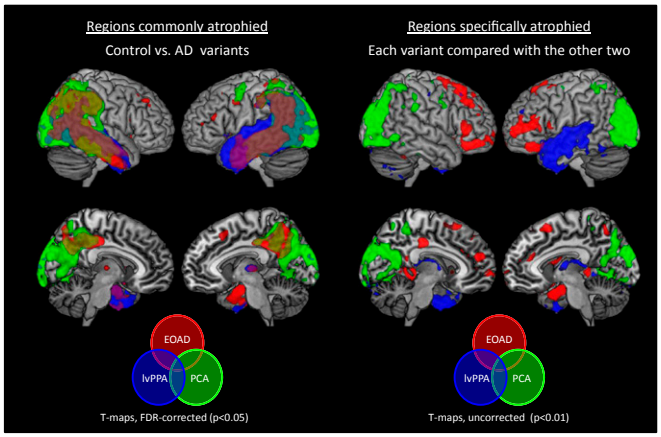

Fig. 4. Patterns of gray matter atrophy in each patient group compared with controls (*Left*, false discovery rate-corrected $P < 0.05$), and specifically in each patient group compared with the other two (*Right*, uncorrected $P < 0.01$).

in the VBM analysis. It should be noted that as the coordinates for the seed ROIs were derived by comparing each syndrome with the other two, the regions involved represent those affected specifically in each variant, and not necessarily those most involved in each variant compared with controls. Together, our findings indicate that the posterior DMN and the precuneus network are core networks commonly affected in AD variants, whereas syndrome-specific patterns of neurodegeneration in AD variants are driven by the involvement of specific functional networks outside the DMN.

Several mechanisms have been postulated to explain the vulnerability of the DMN in AD. Neural activity enhances amyloid-beta (Aβ) production and aggregation (30, 31), which may explain the preferential and early deposition of amyloid in highly interconnected neocortical hubs, many of which are contained in the DMN (32–34). It has also been suggested that the DMN may be more vulnerable to the neurotoxic effects of Aβ because of high metabolic stress (18, 34, 35). Metabolic stress in the DMN has been related to its high interconnectivity and frequent fluctuations between activated and deactivated states (18, 34). The DMN has also been shown to heavily rely on aerobic glycolysis (i.e., glucose use in excess of that used for oxidative phosphorylation), even more than other brain regions that also show high levels of energy consumption (e.g., visual cortex) (36, 37). Neurons from PCC within the DMN show reduced mitochondrial activity in young adults carrying the apolipoprotein E4 gene, reflected by lower mitochondrial cytochrome oxidase activity (38) and lower expression of genes that encode subunits of the mitochondrial electron transport chain in AD compared with controls (35). The DMN may therefore represent a network in which amyloid deposition converges with metabolic vulnerability, rendering it susceptible to early neurodegeneration in AD.

Our data support a central role of the DMN in AD, and in particular, the posterior (parietal-predominant) part, independent of clinical phenotype. The posterior-predominant involvement of the DMN in AD is consistent with a recent functional connectivity study that investigated the modulation of three default mode subnetworks (ventral, anterior, and posterior) in AD (25), showing decreased connectivity in the posterior DMN and increased connectivity in the anterior and ventral DMN in the early symptomatic disease stage. Our data further showed a strong involvement of the precuneus network across AD variants. The precuneus network template partially overlapped the posterior DMN template (20%), which may partly explain the strong association of both networks in the GOF analysis. The precuneus (in particular the ventral precuneus) has been described as one of the most strongly interconnected hubs within the DMN (39) and is activated by a wide spectrum of highly integrative tasks, including visuospatial imagery, episodic memory retrieval, and self-processing operations (40).

Although our data indicate a strong involvement of the posterior DMN and the precuneus network in all three AD variants, the inferior parietal ROI connectivity map also showed a strong fit with the left executive-control network, illustrating the involvement of DMN structures in other functional networks and potentially demonstrating how the DMN could serve as a portal for disease spread into closely interconnected posterior brain regions. Temporoparietal regions that form the core of the posterior DMN are also included in the networks implicated in executive-control, language, and higher-order visual function. The connectivity maps derived from syndrome-specific ROIs in our study suggest that spread of disease from the DMN into distinct posterior networks may drive the clinical phenotype in AD. However, as discussed later in this article, the direction of this spread remains the subject of further investigation. An alternative and equally viable interpretation of our data are that the disease starts in specific "off-target" networks and converges in the posterior DMN.

The connectivity networks derived from common and syndrome-specific ROIs match well with, respectively, the common and variant-specific atrophy patterns found in patients, supporting the hypothesis that neurodegeneration in AD spreads via functional networks. The networks detected from syndrome-specific ROIs closely match the dominant phenotype of each variant. The overlap between the EOAD ROI connectivity map and the executive-control network is consistent with the attention and executive deficits observed in EOAD compared with lvPPA and PCA (41). The overlap between the language network and the lvPPA ROI connectivity map is consistent with the dominant language deficits seen in lvPPA (7). Similarly, the high correspondence of the connectivity map produced by the PCA ROI with the higher visual network is consistent with the visual integration deficits in PCA (6). Importantly, the connectivity data presented here in normal controls converge with a recent PET study in patients with AD that found that distinct patterns of glucose hypometabolism in patients with EOAD, lvPPA, and PCA overlapped with the same network templates (right executive-control, language, and higher visual, respectively) (26).

However, it is also worth pointing out some discrepancies between patterns of functional connectivity and neurodegenerative patterns, as illustrated by the strong involvement of the cerebellum and brainstem in the common networks. Although these regions are not typically atrophied in AD, there is a growing number of studies that report pathological changes in these regions (42–45). The cerebellum and brainstem are also strongly connected to other cortical regions (46–48) and have been implicated as part of several intrinsic networks (22, 49). It is also worth noting that although connectivity studies capture regions that are functionally connected, these may not necessarily overlap with regions affected by neurodegeneration at a certain point in the disease. Functional networks capture polysynaptic pathways, which means that if a disease spreads contiguously from an epicenter through a network, it may not involve the most distant parts of that network until its later stages. Therefore, a region may be included in a connectivity map because it is highly integrated into a network, but it may not necessarily be affected by the disease yet. This may explain the strong involvement of the cerebellum and brainstem in the connectivity maps, even though these regions do not show atrophy early in the course of AD.

The mechanisms by which AD spreads through neural networks are not known. Previous studies from our group and others using amyloid PET have shown that the distribution of fibrillar amyloid in AD is largely overlapping and is indistinguishable across clinical variants (26, 50–53). This raises the possibility that network-based degeneration may be driven by other factors, such as oligomeric Aβ (not imaged by current PET ligands) or neurofibrillary tangles. Although speculative, the possibility of network-based spread of neurofibrillary pathology is particularly compelling, given recent evidence from in vitro assays and animal models that tau spreads transsynaptically through neural circuits (16, 54). Autopsy studies have further shown greater tangle but not amyloid pathology in visual processing regions in PCA (55, 56) and in left-hemisphere language regions in aphasic vs. amnestic AD (8, 57). However, it is also worth pointing out that a brain region may show a loss of function as a result of reduced input from a remote region that is affected by the disease rather than a result of local pathology. Future studies using emerging tau ligands (58) are needed to tease apart these different processes and to evaluate in vivo the relationships between regional tau deposition, neurodegeneration, and clinical phenotype.

To summarize, we propose the following speculative model to explain network-based degeneration in AD (Fig. S3): Amyloid may aggregate throughout highly interconnected cortical hub regions in association neocortex, driven by high neural activity (34), along with decreased clearance in predisposed individuals (59), producing high local concentrations of Aβ. Possibly facilitated by Aβ (60), tau pathology may develop in vulnerable networks, such as the posterior DMN, and then spread transneuronally (15–17)

into closely interconnected networks, including those involved in visuospatial, language, and executive function. This may lead to neurodegeneration in specific functional networks, resulting in heterogeneous clinicoanatomical AD phenotypes. Although this model explains both the central role of the DMN and the clinicoanatomical heterogeneity in AD, it should be noted that there are currently limited data on the direction of the transneuronal spread. In fact, the early clinical symptoms in each variant correlate with functions subserved by the specifically involved networks (executive dysfunction in EOAD, language in lvPPA, and visual integration in PCA), rather than the commonly involved posterior DMN, suggesting that AD pathology in each variant may begin in the respective off-target network and later converge in the DMN. Although a small number of studies have investigated cognitive and structural changes over time in different AD variants (61–65), most of them included patients that were relatively advanced, providing limited information about the early stages of disease.

However, it is also possible that the posterior DMN is less clinically eloquent than the off-target networks. The functional role of the DMN is an area of active investigation. It appears to be activated in a variety of tasks, such as internally focused tasks including autobiographical memory retrieval, envisioning the future, and conceiving the perspectives of others (11, 66). The implications of loss of function are less clear, as this region has not been explored in traditional lesion studies. It may be that the posterior DMN serves more of an integrative role and that loss of function is not apparent as a specific clinical deficit. Furthermore, clinical symptoms are a reflection not only of neurodegeneration but also of cognitive reserve (relating to the ability of a person to compensate for the loss of function in a particular region or network). Individuals may be better able to compensate for posterior DMN disruptions via engagement of other brain networks, whereas disruptions to the off-target networks may lead to more recognizable clinical symptoms. Further studies using longitudinal data and milder cases are required to obtain a better understanding of the origin and spread of pathological changes in AD variants.

Although the current study provides some insight into the involvement of functional networks in AD variants, networks were investigated in healthy individuals only. Further studies in AD variants are required to assess intrinsic connectivity of different networks in symptomatic patients. Studying network dysfunction in patients may also provide important insights into the relationship between neurodegeneration in functional networks and the cognitive deficits seen in patients. Although the seed-based method is a useful and reliable approach to extract networks, the arbitrary choice of the size of the seed may bias connectivity findings toward specific, smaller, or overlapping subsystems, rather than larger, distinct network (67). Spatial normalization errors may also have confounding effects on the data. Using other approaches to assess intrinsic connectivity in the brain (such as independent component analysis or graph theory) may provide additional insights into network dysfunction in AD variants. Although the seeds were selected based on peak coordinates from a single study assessing common and distinct gray matter atrophy across AD variants, the representative atrophy patterns are consistent with the current, independent VBM study, as well as studies from other centers (68–70). Because the study by Migliaccio et al. [from which the seed ROI coordinates were obtained (28)] did not include a late-onset AD group, our analysis was restricted to early-onset variants. Further studies are needed to assess network involvement in the more typical late-onset amnestic AD phenotype.

Finally, although network connectivity represents a plausible mechanism of how heterogeneity emerges in AD, perhaps the more intriguing question is why heterogeneity emerges (i.e., what are the specific genetic, developmental, and environmental risk factors that determine whether an individual with AD develops an amnestic, dysexecutive, language, or visuospatial phenotype?). Future studies addressing these questions may yield novel insights into the mechanisms of this clinically diverse but uniformly devastating disease.

Methods

Subjects. Subjects were selected from the University of California, San Francisco (UCSF), Memory and Aging Center database. All subjects or their assigned surrogate decision-makers provided informed consent, and the study was approved by the UCSF Institutional Review Board for Human Research. Details on inclusion criteria and subject characteristics are provided in *SI Methods*.

Healthy control cohort for connectivity analysis. The study included 131 healthy control participants. Subject demographics were as follows: age, 65.5 ± 3.5 y; 37% men; education, 17.4 ± 1.9 y; Mini Mental State Examination (MMSE), 29.5 ± 0.6; and 30% ApoE ε4 carriers.

AD cohort for VBM analysis. A total of 74 patients with AD (age, 61.7 ± 6.3 y; 49% men; education, 15.8 ± 2.7 y; MMSE, 21.3 ± 6.3, Table S2) were included in this analysis, consisting of 36 patients with EOAD, 18 with lvPPA, and 20 with PCA.

Image Analysis: Functional Connectivity Data. Functional images were acquired on a 3-T Siemens MRI scanner at the Neuroscience Imaging Center, UCSF. Details on image acquisition parameters and preprocessing are provided in *SI Methods*.

Seed-based analysis. Seed ROIs were based on peak atrophy voxels defined in a previous VBM study that identified patterns of atrophy in EOAD, lvPPA, and PCA (28). No patient in that study had a family history suggestive of autosomal dominant AD. The three commonly atrophied regions (peak atrophy voxels across all three variants compared with controls) were the left inferior parietal lobule [Montreal Neurological Institute (MNI) coordinates, −51 −58 37], left precuneus (MNI coordinates, −2 −60 44), and left PCC (MNI coordinates, −2 −33 28). Specifically atrophied regions (peak atrophy in each syndrome compared with the other two) were the right middle frontal gyrus in EOAD (MNI coordinates, 40 42 30), left superior temporal sulcus in lvPPA (MNI coordinates, −56 −40 1), and right middle occipital gyrus in PCA (MNI coordinates, 39 −88 10).

ROIs were created by drawing 4-mm spheres around these peak atrophy voxels (Fig. S2). The average time series from each ROI was then used as a covariate of interest in a whole-brain regression analysis. The voxel-wise *z*-scores in the resulting subject-level intrinsic connectivity maps describes the correlation between each voxel's spontaneous blood-oxygen-level-dependent signal time series and the average time series of all voxels within the seed ROI. Connectivity maps were derived from each ROI in each individual and entered into second-level, random effects analyses to derive group-level connectivity maps for each ROI, correcting for age and sex, performed by the FSL randomize program (5,000 random permutations). Connectivity maps are shown as *P* maps after correction for multiple comparisons [family-wise error (FWE), $P < 0.05$]. Overlap maps were created between the three specifically atrophied seed ROI connectivity maps and the three commonly atrophied seed ROI connectivity maps, with each map thresholded at FWE $P < 0.05$.

Goodness-of-fit. GOF analysis was used to assess correspondence between network connectivity maps and a set of 15 functional network templates (29). See *SI Methods* for more details.

Image Analysis: VBM in Patients with AD. T1-weighted scans were acquired on a 3-T Siemens MRI scanner and 1.5-T Magnetom VISION scanner. VBM was performed using Statistical Parametric Mapping, version 8 (Wellcome Trust Centre for Neuroimaging). Details on the VBM processing are provided in *SI Methods*. A general linear model was used to assess group differences in gray matter volume. The model included diagnosis (controls, EOAD, lvPPA, PCA) as the condition, and age, sex, total intracranial volume, and scanner as covariates, with additional correction for MMSE for the between-patient group comparisons. Pairwise contrasts were performed among the four groups. Resulting T-maps are displayed on an MNI template brain corrected for multiple comparisons using a false discovery rate correction at $P < 0.05$ for the control vs. patient group comparisons, and at uncorrected thresholds at $P < 0.01$ for the comparison of each patient group with the other two.

ACKNOWLEDGMENTS. This work was supported by a grant from Alzheimer's Research UK (to M.L.); National Institute on Aging Grants K23-AG031861 (to G.D.R.), R01AG034570 (to W.J.J.), and P01-AG1972403 and P50-AG023501 (to B.L.M.); the John Douglas French Alzheimer's Foundation (G.D.R.); State of California Department of Health Services Alzheimer's Disease Research Center of California Grant 04-33516 (to B.L.M.); the Hellman Family Foundation (to G.D.R.); and a Hilblom Grant (to B.L.M.), which supports normal aging research at the Memory and Aging Center.

1. Braak H, Braak E (1991) Neuropathological stageing of Alzheimer-related changes. *Acta Neuropathol* 82(4):239–259.
2. Snowden JS, et al. (2007) Cognitive phenotypes in Alzheimer's disease and genetic risk. *Cortex* 43(7):835–845.
3. Galton CJ, Patterson K, Xuereb JH, Hodges JR (2000) Atypical and typical presentations of Alzheimer's disease: A clinical, neuropsychological, neuroimaging and pathological study of 13 cases. *Brain* 123(Pt 3):484–498.
4. Frisoni GB, et al. (2007) The topography of grey matter involvement in early and late onset Alzheimer's disease. *Brain* 130(Pt 3):720–730.
5. Koedam EL, et al. (2010) Early-versus late-onset Alzheimer's disease: More than age alone. *J Alzheimers Dis* 19(4):1401–1408.
6. Crutch SJ, et al. (2012) Posterior cortical atrophy. *Lancet Neurol* 11(2):170–178.
7. Gorno-Tempini ML, et al. (2008) The logopenic/phonological variant of primary progressive aphasia. *Neurology* 71(16):1227–1234.
8. Mesulam M, et al. (2008) Alzheimer and frontotemporal pathology in subsets of primary progressive aphasia. *Ann Neurol* 63(6):709–719.
9. McKhann GM, et al. (2011) The diagnosis of dementia due to Alzheimer's disease: Recommendations from the National Institute on Aging-Alzheimer's Association workgroups on diagnostic guidelines for Alzheimer's disease. *Alzheimers Dement* 7(3):263–269.
10. Dubois B, et al. (2010) Revising the definition of Alzheimer's disease: A new lexicon. *Lancet Neurol* 9(11):1118–1127.
11. Greicius MD, Krasnow B, Reiss AL, Menon V (2003) Functional connectivity in the resting brain: A network analysis of the default mode hypothesis. *Proc Natl Acad Sci USA* 100(1):253–258.
12. Fox MD, et al. (2005) The human brain is intrinsically organized into dynamic, anticorrelated functional networks. *Proc Natl Acad Sci USA* 102(27):9673–9678.
13. Seeley WW, Crawford RK, Zhou J, Miller BL, Greicius MD (2009) Neurodegenerative diseases target large-scale human brain networks. *Neuron* 62(1):42–52.
14. Zhou J, Gennatas ED, Kramer JH, Miller BL, Seeley WW (2012) Predicting regional neurodegeneration from the healthy brain functional connectome. *Neuron* 73(6): 1216–1227.
15. Clavaguera F, et al. (2009) Transmission and spreading of tauopathy in transgenic mouse brain. *Nat Cell Biol* 11(7):909–913.
16. de Calignon A, et al. (2012) Propagation of tau pathology in a model of early Alzheimer's disease. *Neuron* 73(4):685–697.
17. Frost B, Jacks RL, Diamond MI (2009) Propagation of tau misfolding from the outside to the inside of a cell. *J Biol Chem* 284(19):12845–12852.
18. Buckner RL, et al. (2005) Molecular, structural, and functional characterization of Alzheimer's disease: Evidence for a relationship between default activity, amyloid, and memory. *J Neurosci* 25(34):7709–7717.
19. Greicius MD, Srivastava G, Reiss AL, Menon V (2004) Default-mode network activity distinguishes Alzheimer's disease from healthy aging: Evidence from functional MRI. *Proc Natl Acad Sci USA* 101(13):4637–4642.
20. Mormino EC, et al. (2011) Relationships between β-amyloid and functional connectivity in different components of the default mode network in aging. *Cereb Cortex* 21(10):2399–2407.
21. Petrella JR, Sheldon FC, Prince SE, Calhoun VD, Doraiswamy PM (2011) Default mode network connectivity in stable vs progressive mild cognitive impairment. *Neurology* 76(6):511–517.
22. Zhou J, et al. (2010) Divergent network connectivity changes in behavioural variant frontotemporal dementia and Alzheimer's disease. *Brain* 133(Pt 5):1352–1367.
23. Raichle ME, et al. (2001) A default mode of brain function. *Proc Natl Acad Sci USA* 98(2):676–682.
24. Gusnard DA, Akbudak E, Shulman GL, Raichle ME (2001) Medial prefrontal cortex and self-referential mental activity: Relation to a default mode of brain function. *Proc Natl Acad Sci USA* 98(7):4259–4264.
25. Damoiseaux JS, Prater KE, Miller BL, Greicius MD (2012) Functional connectivity tracks clinical deterioration in Alzheimer's disease. *Neurobiol Aging* 33(4):828.e19–e30.
26. Lehmann M, et al. (2013) Diverging patterns of amyloid deposition and hypometabolism in clinical variants of probable Alzheimer's disease. *Brain* 136(Pt 3):844–858.
27. Lehmann M, et al. (2010) Reduced cortical thickness in the posterior cingulate gyrus is characteristic of both typical and atypical Alzheimer's disease. *J Alzheimers Dis* 20(2): 587–598.
28. Migliaccio R, et al. (2009) Clinical syndromes associated with posterior atrophy: Early age at onset AD spectrum. *Neurology* 73(19):1571–1578.
29. Shirer WR, Ryali S, Rykhlevskaia E, Menon V, Greicius MD (2012) Decoding subject-driven cognitive states with whole-brain connectivity patterns. *Cereb Cortex* 22(1): 158–165.
30. Bero AW, et al. (2011) Neuronal activity regulates the regional vulnerability to amyloid-β deposition. *Nat Neurosci* 14(6):750–756.
31. Cirrito JR, et al. (2005) Synaptic activity regulates interstitial fluid amyloid-beta levels in vivo. *Neuron* 48(6):913–922.
32. Mintun MA, et al. (2006) [11C]PIB in a nondemented population: Potential antecedent marker of Alzheimer disease. *Neurology* 67(3):446–452.
33. Mormino EC, et al.; Alzheimer's Disease Neuroimaging Initiative (2009) Episodic memory loss is related to hippocampal-mediated beta-amyloid deposition in elderly subjects. *Brain* 132(Pt 5):1310–1323.
34. Buckner RL, et al. (2009) Cortical hubs revealed by intrinsic functional connectivity: Mapping, assessment of stability, and relation to Alzheimer's disease. *J Neurosci* 29(6):1860–1873.
35. Liang WS, et al. (2008) Alzheimer's disease is associated with reduced expression of energy metabolism genes in posterior cingulate neurons. *Proc Natl Acad Sci USA* 105(11):4441–4446.
36. Vlassenko AG, et al. (2010) Spatial correlation between brain aerobic glycolysis and amyloid-β (Aβ) deposition. *Proc Natl Acad Sci USA* 107(41):17763–17767.
37. Vaishnavi SN, et al. (2010) Regional aerobic glycolysis in the human brain. *Proc Natl Acad Sci USA* 107(41):17757–17762.
38. Valla J, et al. (2010) Reduced posterior cingulate mitochondrial activity in expired young adult carriers of the APOE ε4 allele, the major late-onset Alzheimer's susceptibility gene. *J Alzheimers Dis* 22(1):307–313.
39. Zhang S, Li CS (2012) Functional connectivity mapping of the human precuneus by resting state fMRI. *Neuroimage* 59(4):3548–3562.
40. Cavanna AE, Trimble MR (2006) The precuneus: A review of its functional anatomy and behavioural correlates. *Brain* 129(Pt 3):564–583.
41. Smits LL, et al. (2012) Early onset Alzheimer's disease is associated with a distinct neuropsychological profile. *J Alzheimers Dis* 30(1):101–108.
42. Braak H, Del Tredici K (2011) Alzheimer's pathogenesis: Is there neuron-to-neuron propagation? *Acta Neuropathol* 121(5):589–595.
43. Grinberg LT, et al.; Brazilian Brain Bank Study Group (2009) The dorsal raphe nucleus shows phospho-tau neurofibrillary changes before the transentorhinal region in Alzheimer's disease. A precocious onset? *Neuropathol Appl Neurobiol* 35(4):406–416.
44. Parvizi J, Van Hoesen GW, Damasio A (2001) The selective vulnerability of brainstem nuclei to Alzheimer's disease. *Ann Neurol* 49(1):53–66.
45. Simic G, et al. (2009) Does Alzheimer's disease begin in the brainstem? *Neuropathol Appl Neurobiol* 35(6):532–554.
46. O'Reilly JX, Beckmann CF, Tomassini V, Ramnani N, Johansen-Berg H (2010) Distinct and overlapping functional zones in the cerebellum defined by resting state functional connectivity. *Cereb Cortex* 20(4):953–965.
47. Ramnani N (2006) The primate cortico-cerebellar system: Anatomy and function. *Nat Rev Neurosci* 7(7):511–522.
48. Hurley RA, Flashman LA, Chow TW, Taber KH (2010) The brainstem: Anatomy, assessment, and clinical syndromes. *J Neuropsychiatry Clin Neurosci* 22(1):iv–, 1–7.
49. Habas C, et al. (2009) Distinct cerebellar contributions to intrinsic connectivity networks. *J Neurosci* 29(26):8586–8594.
50. Rosenbloom MH, et al. (2011) Distinct clinical and metabolic deficits in PCA and AD are not related to amyloid distribution. *Neurology* 76(21):1789–1796.
51. de Souza LC, et al. (2011) Similar amyloid-β burden in posterior cortical atrophy and Alzheimer's disease. *Brain* 134(Pt 7):2036–2043.
52. Rabinovici GD, et al. (2010) Increased metabolic vulnerability in early-onset Alzheimer's disease is not related to amyloid burden. *Brain* 133(Pt 2):512–528.
53. Leyton CE, et al. (2011) Subtypes of progressive aphasia: Application of the International Consensus Criteria and validation using β-amyloid imaging. *Brain* 134(Pt 10):3030–3043.
54. Liu L, et al. (2012) Trans-synaptic spread of tau pathology in vivo. *PLoS ONE* 7(2): e31302.
55. Renner JA, et al. (2004) Progressive posterior cortical dysfunction: A clinicopathologic series. *Neurology* 63(7):1175–1180.
56. Tang-Wai DF, et al. (2004) Clinical, genetic, and neuropathologic characteristics of posterior cortical atrophy. *Neurology* 63(7):1168–1174.
57. Gefen T, et al. (2012) Clinically concordant variations of Alzheimer pathology in aphasic versus amnestic dementia. *Brain* 135(Pt 5):1554–1565.
58. Chien DT, et al. (2013) Early clinical PET imaging results with the novel PHF-tau radioligand [F-18]-T807. *J Alzheimers Dis* 34(2):457–468.
59. Mawuenyega KG, et al. (2010) Decreased clearance of CNS beta-amyloid in Alzheimer's disease. *Science* 330(6012):1774.
60. Chabrier MA, et al. (2012) Soluble aβ promotes wild-type tau pathology in vivo. *J Neurosci* 32(48):17345–17350.
61. Rohrer JD, et al. (2013) Patterns of longitudinal brain atrophy in the logopenic variant of primary progressive aphasia. *Brain Lang*, 10.1016/j.bandl.2012.12.008.
62. Leyton CE, Hsieh S, Mioshi E, Hodges JR (2013) Cognitive decline in logopenic aphasia: More than losing words. *Neurology* 80(10):897–903.
63. Lehmann M, et al. (2012) Global gray matter changes in posterior cortical atrophy: A serial imaging study. *Alzheimers Dement* 8(6):502–512.
64. Kennedy J, et al. (2012) Visualizing the emergence of posterior cortical atrophy. *Neurocase* 18(3):248–257.
65. Cho H, et al. (2013) Longitudinal changes of cortical thickness in early- versus late-onset Alzheimer's disease. *Neurobiol Aging* 34(7):1921.e9–1921-1921.e9.15.
66. Buckner RL, Andrews-Hanna JR, Schacter DL (2008) The brain's default network: Anatomy, function, and relevance to disease. *Ann N Y Acad Sci* 1124:1–38.
67. Cole DM, Smith SM, Beckmann CF (2010) Advances and pitfalls in the analysis and interpretation of resting-state FMRI data. *Front Syst Neurosci* 4:8.
68. Ridgway GR, et al. (2012) Early-onset Alzheimer disease clinical variants: Multivariate analyses of cortical thickness. *Neurology* 79(1):80–84.
69. Whitwell JL, et al. (2007) Imaging correlates of posterior cortical atrophy. *Neurobiol Aging* 28(7):1051–1061.
70. Sapolsky D, et al. (2010) Cortical neuroanatomic correlates of symptom severity in primary progressive aphasia. *Neurology* 75(4):358–366.